GEOLOGICA CARPATHICA, APRIL 2021, 72, 2, 155–169 https://doi.org/10.31577/GeolCarp.72.2.5

Manganese-rich carbonate and phosphate concretions from the Subsilesian Unit of the Outer Western Carpathians (Czech Republic): Composition and unique selenium weathering products

DALIBOR MATÝSEK[1] and JAKUB JIRÁSEK[2,✉]

[1]VŠB – Technical University of Ostrava, Faculty of Mining and Geology, Department of Geological Engineering, 17. listopadu 15/2172, 708 33 Ostrava-Poruba, Czech Republic; dalibor.matysek@vsb.cz
[2]University Olomouc, Faculty of Science, Department of Geology, 17. listopadu 1192/12, 771 46 Olomouc, Czech Republic; ✉jakub.jirasek@upol.cz

(Manuscript received December 2, 2020; accepted in revised form March 24, 2021; Associate Editor: Igor Broska)

Abstract: This research focuses on two new occurrences of sedimentary concretions in the Subsilesian Unit of the Outer Western Carpathians (Czech Republic) from non-calcareous clays and claystones of the Paleocene to the Eocene age. Powder X-ray diffraction study proved heterogenous matrix, varying in content of siderite, Mn-rich siderite, Ca-rich rhodochrosite and fluorapatite. Electron microscopy revealed microsparitic carbonates with indistinct zoning. According to the geochemical and stable isotope clues the concretions originated in medium to highly reducting environment during early diagenesis. Stable isotope $\delta^{13}C$ values (−11.3 and −4.8 ‰ PDB) and $\delta^{18}O$ (1.8 and 1.0 ‰ PDB) correspond well to early diagenetic marine carbonates and part of the CO_2 was derived from oxidation of biological material. Weathering of concretions has been on the surface and along fissures. While siderite-rich concretions produce goethite, rhodochrosite-rich concretions produce a cellular structure of todorokite, birnessite and *buserite* on rims of carbonate cores. Fissure mineralisation contains association of goethite accompanied by native selenium and clausthalite. The origin of the selenium minerals is interpreted as products on the redox barrier between Mn^{2+}/Mn^{4+} and/or Fe^{2+}/Fe^{3+}, where selenites and selenates are highly soluble but native selenium and selenides are extremely insoluble.

Keywords: Outer Carpathians, Tertiary, carbonate concretions, mineralogy, petrology, selenium, clausthalite.

Introduction

Carbonate, especially siderite but also dolomite, calcite and, rarely, rhodochrosite concretions and nodules (terminology after Sellés-Martínez 1996) or lens-like layers, are a common part of sedimentary sequences of marine or lake origin (Dietrich 1999a,b). Since they are a seemingly foreign component by their shape and manner of occurrence, they attract attention as a frequent subject of studies (Dale et al. 2014; Mavromatis et al. 2014; Plet et al. 2016; Kamran et al. 2020). Despite hundreds of published papers devoted to concretions in sediments, it is not possible to consider all aspects of their formation fully understood. The composition of carbonate nodules can provide interesting information about processes occurring in sediments.

Even on a global scale, carbonate nodules with a high proportion of a manganese component (i.e., rhodochrosite or Ca-rich rhodochrosite nodules) are not as common as those formed by other carbonates. They are exemplified by Morad & Al-Aasm (1997), Hodgson (1968), Nakada et al. (2014) and others.

Carbonate concretions are usually formed during diagenetic processes in their early stages, when the sediment undergoes gradual decomposition of contained organic matter (Sellés-Martínez 1996). This decomposition is probably mediated microbially (De Craen et al. 1999; Baumann et al. 2016) and associated with methanogenesis (Bojanowski & Clarkson 2012), with the reduction of sulphates to H_2S, trivalent Fe^{3+} to divalent Fe^{2+}, as well as the formation of simple organic acids and CO_3^{2-}. Thus, in sediments near the surface, supersaturation of pore waters with carbonates of divalent ions and the sediment fulfils the thermodynamic assumption of crystallisation of carbonates (Yoshida et al. 2018).

The aims of the study were to draw attention to the mineralogical variability of the Outer Carpathian concretions from non-calcareous clays and claystones of the Paleocene to the Eocene age, to reveal their genesis and their unusual weathering products.

Geological setting

Outer Western Carpathians

The Outer Carpathians represent the most external zone of the Carpathian mountain belt. The study area lies at its NW edge ca. 5 km from the front of the Carpathian nappes. The Outer Carpathians comprise a structurally complex area

that consists of folded and thrusted strata in age Late Jurassic to the Late Miocene. In their present form, the Outer Western Carpathians consist of two groups of nappes: the lower Outer Group (from lowest to highest part the Subsilesian, Silesian and Ždánice nappes) and the upper Magura Group (Rača, Bílé Karpaty and Bystrica nappes; see Fig. 1). The whole nappe allochthon is thrust more than 60 km over the Miocene sediments of the Carpathian Foredeep (Picha et al. 2006).

The north to north-western part of the Waschberg–Ždánice–Subsilesian Unit is designated as a Subsilesian Unit (Nappe). It contains sediments from the Turonian to the Oligocene. In the sedimentary fill, clays and claystones predominate over occasional sandstones. Gravitational subaqueous slide bodies formed by paraconglomerates frequently occur in the whole sequence. Eliáš (1998) and Menčík et al. (1983) recognised four basic lithostratigraphical units: (1) the Frýdek Formation (Turonian–Maastrichtian) is coposed of gray or black-gray calcareous claystones with an estimated thickness ca. 500 m; especially in the youngest parts, there are intercalations of sandstones to conglomerates; (2) the Frýdlant Formation (Paleocene–Eocene) contains mainly facially very variable claystones like black-gray claystones, speckled claystones, variegated claystones and also sandy facies, with an estimated thickness of ca. 800 m; (3) the Menilite Formation (Oligocene) consists of aleuropelites with silicite intercalations and marlstone in the youngest parts, with a thickness up to 100 m and (4), on top the poorly recognised Ženklava Formation (Oligocene–Early Miocene) is present. Large facial variability can be expected from paleogeographic variability, especially in the Subsilesian Unit.

Phosphate and Mn-rich carbonate concretions in Outer Carpathians

In the sediments of the Outer Western Carpathians, mineralogy and geochemistry of carbonate and concretions or layers were studied only marginally. The diagenetic nodules and layers were studied only in the Silesian Unit, despite the fact that they were subjected to intensive mining, mainly during the first half of the 19th century. The lenticularly developed beds of sedimentary siderites from the Hradiště and Lhoty formations of the Silesian Unit in the foothills of the Moravian–Silesian Beskydy Mine were even exploited. A summary of historical knowledge of siderite carbonates of the Silesian Unit is provided by Roth & Matějka (1953).

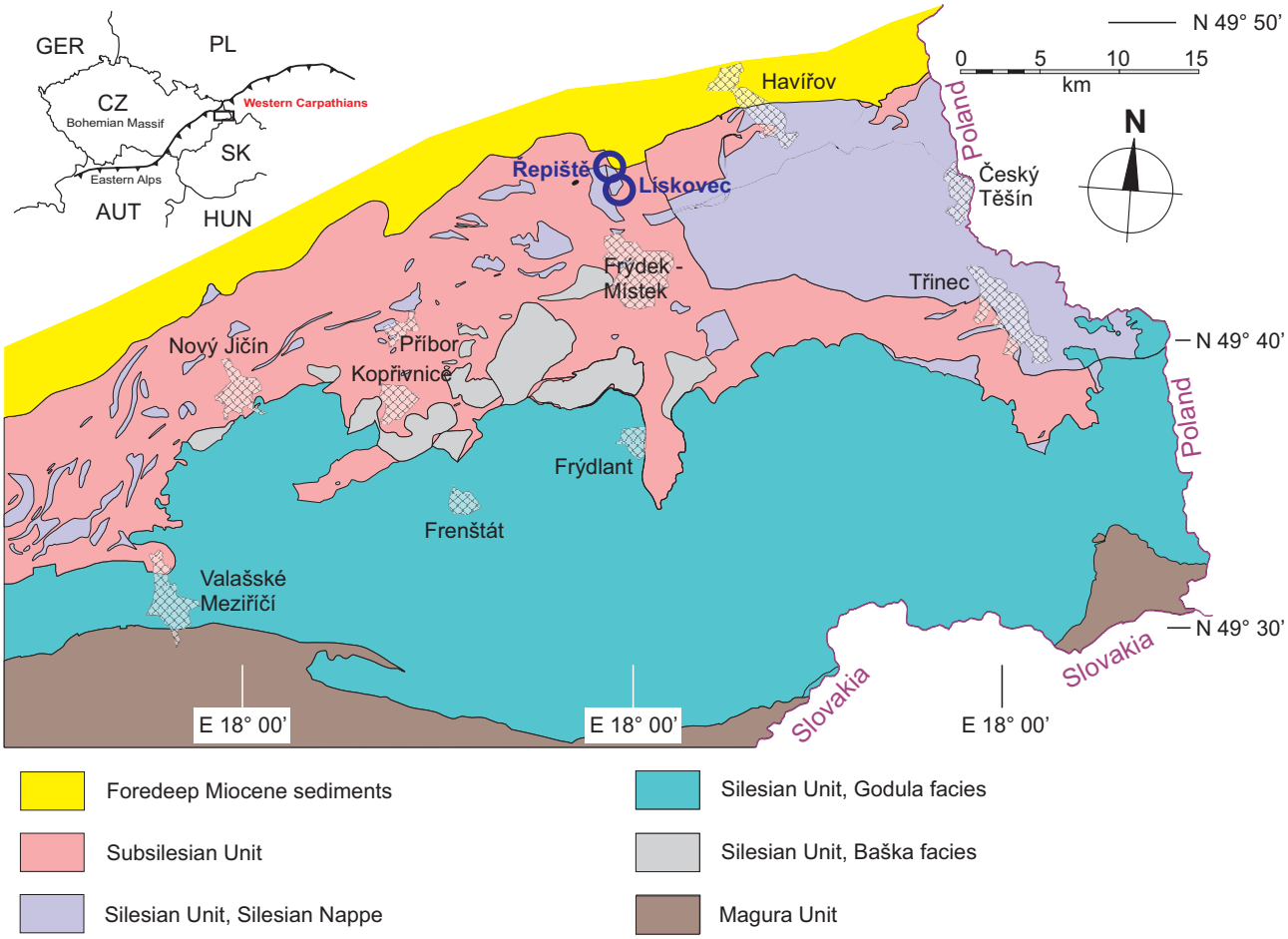

Fig. 1. Schematic geological map of the Czech northern part of the Outer Western Carpathians with the position of the studied localities (according to Matýsek et al. 2018, modified).

The manganese is noticeably high in concretions from various stratigraphic and structural tectonic units of the Polish part of the Outer Carpathians. Gucwa & Wieser (1978) divided them into four types: (a) a small goethite–todorokite–birnessite nodule with a compact structure; (b) large goethite± pyrolusite and hematite nodules with cellular structure that are secondary after *oligonite* (i.e., Mn-rich siderite); (c) large *oligonite*, Ca-rich rhodochrosite or mixed nodules with compact structures and (d) phosphate nodules, which are referred to as *francolite* or *francolite*–rhodochrosite nodules with compact structures.

Jasionowicz et al. (1959) and Narębski (1960) investigated abundant phosphate concretions from the varied marlstones of the Upper Cretaceous (Węglowiec Member, Maastrichtian to Danian, Trepcza site near Sanok, SE Poland). According to chemical analysis, concretions are the intermediate member of the fluorapatite–hydroxylapatite series containing $(CO_3)^{2-}$ group. From the Eocene sedimentary sequence of the Skole Unit (variegated shales and hieroglyphic beds), Muszyński et al. (1978) reported the occurrence of Ca-rich rhodochrosite, Ca–Mg-rich rhodochrosite to Ca-*pistomesite* (i.e., Ca–Mg-rich siderite). From the same area, similar carbonate micronodules composed of rhodochrosite with various Ca and Fe content were described by Wieser (1982).

The occurrence of concrecional phosphate containing rhodochrosite was reported by Matýsek & Skupien (2005) from the Silesian Unit (lower section of the Godula Formation) from the locality Bystrý potok near Kunčice pod Ondřejníkem. From the Frýdek Formation (Maastrichtian–Paleocene) of the Lower Silesian Unit, Matýsek & Bubík (2012) reported phosphate and siderite concretions. They interpret phosphates as possible coprolites. Ironically, the manganese-rich carbonate nodules from the Subsilesian unit were probably described already by Moser (1875). He referred to *Brauneisenerz* (obsolete German name for iron oxides/hydroxydes) as a nodular, siderite-like grey layer, covered with a black coating, of the red-coloured Eocene layers from Lubno and Nová Ves near Frýdlant. However, this occurrence was not revised in the later times by modern techniques.

Mineralogy of carbonate concretions from Silesian Unit have recently was dealt by Dziubińska & Narębski (2004), Buriánek et al. (2011) and Bojanowski (2014). Dziubińska & Narębski (2004) stated that siderite is the main constituent of concretions, with dolomite, Fe-rich dolomite and calcite being less common. They further state that the first phase that crystallises from the pore solutions is carbonate enriched mainly with manganese. The authors thus interpret the zoning of siderite crystals, where the central parts of the crystals are enriched with Mn, Ca and Mg and the margins are significantly enriched with Fe. The authors present a variation range of the composition of the edges of siderite crystals: $(Fe_{0.54–0.80}Mg_{0.11–0.23}Ca_{0.05–0.135}Mn_{0.005–0.11})CO_3$ and centres $(Fe_{0.4–0.65}Mg_{0.085–0.14}Ca_{0.085–0.13}Mn_{0.18–0.37})CO_3$. Obviously, the siderites are strongly substituted and, according to the authors, correspond to the *sideroplesites* and *manganospherites*. They are of early diagenetic origin and depleted of all trace elements except Sr.

Buriánek et al. (2011) studied three concretions of the Silesian Unit (Veřovice and Istebná members and Albian–Cenomanian of the Kelč Development). Concretions are up to 1 meter in size, consisting of siderite with composition $(Fe_{0.56–0.8}Ca_{0.03–0.07}Mg_{0.09–0.19}Mn_{0.01–0.06})CO_3$ and contain also accessory calcite and framboidal pyrite. The authors mention irregular zoning in siderite, with enrichment of Si and Al in the crystal centres. They also found significant differences in siderite particle size of nodules.

Bojanowski (2014) reported the occurrence of a concretional authigenic dolomite from the Oligocene to the Eocene of the Dukla and Grzybow units. According to the isotopic composition, the main source of CO_2 is microbial methanogenesis. Dolomite crystals are zoned; the author separated dolomite, Fe-rich dolomite and ankerite from the centre of the crystals, but according to the valid IMA terminology it is also a Fe-rich dolomite. Siderites with an occasionally increased proportion of a rhodochrosite component have been reported in the Soláň Formation of the Račany Unit (Dolníček et al. 2019).

Material

Concretions occurring as a component of river sediments in small watercourses on the western slope of the Řepiště Plateau, south of Ostrava, were studied. Due to the low lithification of the sediments of the Subsilesian Unit (the predominant rocks are wet, expansive clays or claystones), it is exceptional to observe these concretions in the sedimentary sequence in-situ. The Řepiště Plateau is the geomorphological structure on the southern edge of the Ostrava Basin covered by Saalian (Quaternary) glacilacustrine clays and sands and loess clays (Macoun et al. 1965). Small streams draining the erosion slopes of this plateau pass through the Quaternary sediments up to the base, which is formed by sediments of the Subsilesian and Silesian units. The concretions from the small, periodically drying watercourse, located on the cadastre of the village **Řepiště** in the forest called Zaryje, were studied in detail (GPS coordinates 49°44.541' N, 18°18.436' E, Fig. 1). In the geological map of the Czech Geological Survey 1:50,000 (Macoun 1989) sediments of the Frýdek Formation are reported in the area, but only samples from the lower part of the watercourse – beige-grey sandy, laminated, strongly calcareous clays to claystones – correspond to them. In the middle part of the watercourse, there are light green-grey, brown-banded clays, which are non-calcareous, damp-plastic, and after drying and subsequent wetting, strongly deteriorating. The clays are clearly affected by both solifluction and tectonics. According to lithology, these sediments correspond to the lower part of the Frýdlant Formation (Eliáš 1998; Bubík et al. 2016). In the upper part of the watercourse, there are imperfectly uncovered residues of gravels of the main terrace (or so-called gravels of the Řepiště Plateau; Macoun et al. 1965), sandy glaciolacustrine clays with occasional glacial erratics and, in uppermost parts, loess loam.

The concretions are very variable in shape and quite abundant in the locality. Smaller nodules are spherical to ovoid (Fig. 2), 5–10 cm large, with a smooth light grey coloured surface, which, apparently due to oxidation of manganese in the aqueous environment, is gradually covered with a black coating. In the case of uncoated nodules, the inner mass is coloured light greenish-grey or beige to brownish grey and is massive, without macroscopically recognisable grains (Fig. 2B,C). More often, the nodules are slightly weathered. These tend to be beige to rust brown and contain abundant black or rust cracks on the fissures (Fig. 2A,D). In addition, there are also large-sized nodules, up to 40 cm in size and disc-shaped. Septarian cracks filled with calcite were rarely detected. The concretions were also studied on a locality in the notch of a nameless brook in the northern part of the cadastre of **Líškovec** near Frýdek-Místek (GPS 49°43.366' N, 18°18.896' E, Fig. 1). The concretions come from pale greenish-grey, slushy claystones to clays. The layer of the brick-red claystone, which points to the variegated facies of the Frýdlant Formation. was identified on site. Local concretions are relatively large (longer axis up to about 40 cm) and are ovoid to spherical with a smooth surface. The inner mass is light greenish grey to greyish-white, with rather abundant traces of bioturbation. Concretions do not contain septarian cracks, but there are rarely transverse cracks filled by calcite. Weathering usually produces *limonite* (Fig. 3).

Methods

Concretion samples were studied by powder X-ray diffraction (PXRD) analysis and electron microanalysis (EPMA). Bulk chemical analysis and isotopic composition of carbonates was investigated on selected samples from the locality Řepiště.

Powder X-ray diffraction analyses were carried out using a Bruker-AXS D8 Advance instrument with a 2θ/θ measurement geometry and the positionally sensitive detector LynxEye under the following conditions: radiation CuKα/Ni filter, current 40 kV, 40 mA voltage, step mode with a step of 0.014° 2θ, and a total time of 15 seconds per step. Analysis of diffraction

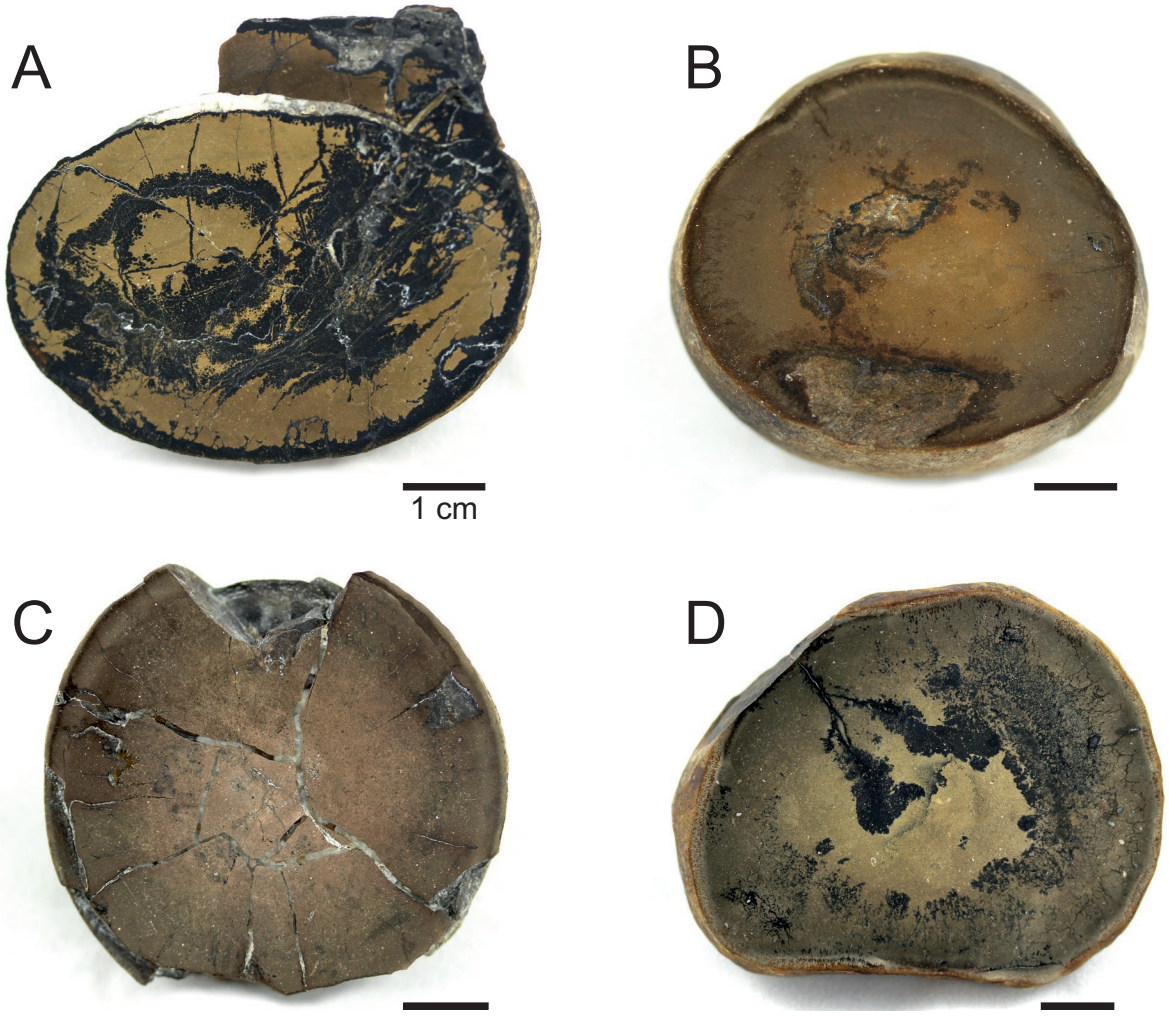

Fig. 2. Polished sections of concretions from the Řepiště locality. Matrix: **A** — rhodochrosite; **B**, **C** — rhodochrosite–phosphate; **D** — phosphate. Black coatings and impregnations represent manganese oxides, white mineral in the septarian cracks is calcite.

patterns was performed using the EVA software (Bruker-AXS) and the database PDF-2, release 2011 (International Centre for Diffraction Data). The Rietveld method using the TOPAS software, version 4.2 (Bruker) was applied to verify the semi-qualitative analyses.

Microscopic investigation and energy-dispersive X-ray spectroscopy (EDS) microanalysis were carried out on an electron microscope FEI Quanta 650 FEG. Analyses were made using both polished thin sections and natural fracture surfaces that were coated with a 35 nm thin film of Cr or 50 nm thin film of C under the following conditions: 15 kV beam voltage, 8–10 nA current, 5 to 6 μm beam diameter, and a vacuum $<10^{-3}$ Pa. Identification and quantification of spectral lines was performed using the decomposition method by means of halographic peak deconvolution. Photomicrographs were taken with a backscattered electron detector (BSE) in chemical gradient mode.

Chemical composition of carbonates was studied with an electron microprobe Cameca SX 100 at the Faculty of Science, Masaryk University in Brno (analyst R. Škoda). The following conditions were used: wavelength-dispersive analysis (WDS), accelerating voltage 15 keV, beam current 10 nA, beam diameter 5 μm. Well defined minerals and synthetic phases were used as standards: sanidine (Si Kα, Al Kα, K Kα), spessartine (Mn Kα), forsterite (Mg Kα), albite (Na Kα), $SrSO_4$ (Sr Lα), almandine (Fe Kα), wollastonite (Ca Kα), baryte (Ba Lα), gahnite (Zn Kα), topaz (F Kα), and vanadinite (Pb Mα). Raw intensities were corrected for matrix effects using the *X-PHI* algorithm (Merlet 1994).

Combined use of EDS and WDS analysis of carbonates proved useful. Comparison of both methods allows to support the EDS results (more accurate in case of lighter elements due to smaller energy which not evaporate sample too rapidly), with WDS, more accurate with medium and heavy elements.

Bulk chemical analyses are from three selected samples of concretions (REP-a, REP-b, REP-c) from Řepiště locality and one sample of surrounding claystone (REP-d); each weighed approximately 100 g. The chemical analyses were performed at the Bureau Veritas Mineral Laboratories in Vancouver, Canada. The samples were crushed, pulverized to 200 mesh and reduced in weight by quartering. Aliquots for analyses of the standard oxides were dissolved in hot (95 °C) aqua regia and analyzed using Inductively Coupled Plasma Optical Emission Spectroscopy (ICP-OES). Other elements were analyzed using Inductively Coupled Plasma Mass Spectroscopy (ICP-MS) with another sample aliquot, which was decomposed by lithium borate fusion followed by digestion in diluted (5 %) nitric acid. The carbon and sulfur content of the samples were measured with a LECO analyzer. Loss on ignition (LOI) was used to find the weight difference before and after ignition at 1000 °C. Method detection limits (MDL) are as following: Fe_2O_3 – 0.04 %; SiO_2, Al_2O_3, MgO, CaO, Na_2O, K_2O, TiO_2, P_2O_5, MnO – 0.01 %; Cr_2O_3 – 0.002 %; V – 8 ppm; Ba, Be, Sc, Sn, Zn – 1 ppm; Au, As, Ga, Se, Sr, W – 0.5 ppm; Nd – 0.3 ppm; Co, Th – 0.2 ppm; Ag, Bi, Cd, Ce, Cs, Cu, Hf, La, Mo, Nb, Ni, Pb, Rb, Sb, Ta, Tl, U, Y, Zr – 0.1 ppm; Dy, Gd, Sm, Yb – 0.05 ppm; Er – 0.03 ppm; Eu, Ho, Pr, TOT/C, TOT/S – 0.02 ppm; Hg, Lu, Tb, Tm – 0.01 ppm.

Fig. 3. Concretion from the Lískovec locality with prevailing Mn-rich siderite.

Isotopic ratios of $\delta^{13}C$ and $\delta^{18}O$ of carbonate concretions were determined using the standard methodology for carbonates in the Laboratory of Stable Isotopes of the Czech Geological Survey. The samples were decomposed in H_3PO_4 at 25 °C (a sample with rhodochrosite predominance), respectively at 100 °C (siderite-rich sample). The equilibration time was 24 hours and the generated gas was then analyzed by mass spectrometer. Friedman & O'Neil (1977) correction was applied to rhodochrosite specimen, Rosenbaum & Sheppard (1986) siderite-rich specimen. Results of isotope analyses are conventionally expressed in delta (δ) notation as per mil (‰) deviation from the commonly used PDB (Peedee Belemnite) and SMOW (Standard Mean Ocean Water) standards. Uncertainty involving the whole analytical procedure is better than ±0.3 ‰.

Results

Mineralogy of the concretions

The powder X-ray diffraction analysis of the concretions from the locality **Řepiště-Zaryje** showed that although they look macroscopically and microscopically similar, their carbonate component is very heterogeneous. The individual samples also vary in the content of an apatite component. Two types of concretions were distinguished by the PXRD – *oligonite*-type siderite dominated and concretions formed by mixed rhodochrosite and apatite (apparently fluorapatite), with variable portions of both components. In the **Lískovec** locality, concretions formed by Mn-rich siderite prevail, but we also found some nearly pure siderite ones. Only two individual concretions from this locality yielded apatite, resp. rhodochrosite–apatite composition.

A detailed analysis of the diffraction data of the concretions matrix from both sites shows that neither siderite nor rhodochrosite are present in the samples as a homogeneous phase, but both minerals are mixtures of several, usually two to three, very close components. This is clear by the distinctly atypical, asymmetric shape of the diffraction lines. This is evident from Fig. 4, where the decomposition of the diffraction line (104) is shown for two samples. Carbonate in both the siderite and the apatite-containing rhodochrosite samples can be divided into three phases, with one component (siderite 3) evidently showing wider diffraction lines, i.e. smaller crystal domain sizes. The differences in unit-cell parameters of individual rhodochrosite and siderite phases are not large. For carbonates of general composition belonging to the series of calcite–siderite–rhodochrosite, is not possible from the diffraction data, or from the unit-cell parameters, to unambiguously determine which isomorphic substituent causes these differences. As an admixtures, quartz, albitic plagioclase, mica minerals and chlorite in the concretions were detected.

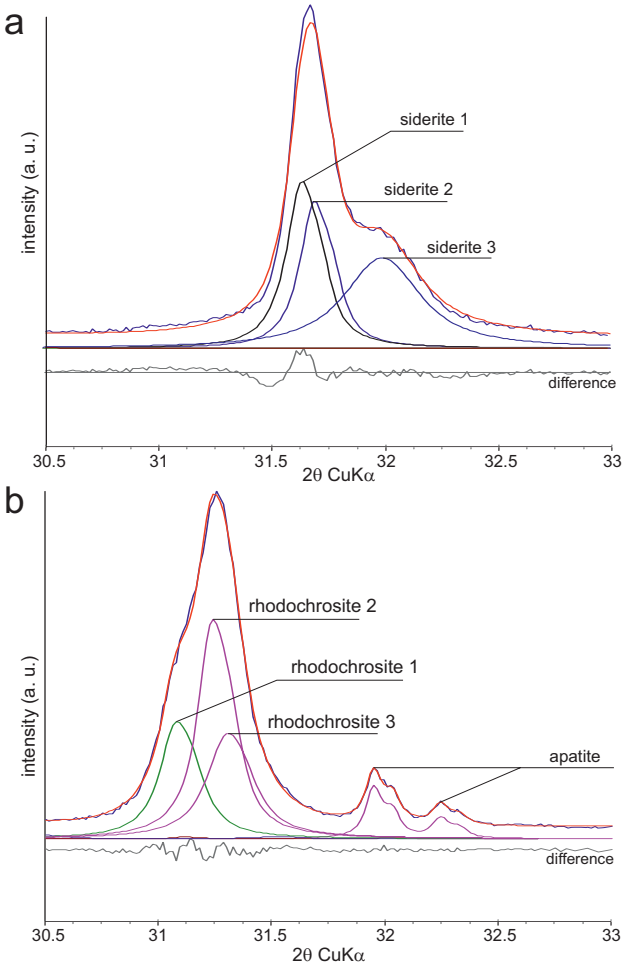

Fig. 4. Decomposition of the diffraction line (104) of the carbonate component in two samples of concretions from the locality Řepiště. Sample **a** represents manganese-rich sideritic carbonate concretion, sample **b** presents rhodochrosite–phosphate carbonate concretion.

The apatite unit-cell parameters range in the interval of a_o=9.3601–9.3617 Å and c_o=6.8897–6.8922 Å and these data are lower than typical fluorapatite and significantly lower than hydroxylapatite. The closest values to fluorapatite reported Comodi et al. (2001) at 9.375 and 6.887 Å. The reason for an imperfect fit may be an isomorphic admixtures (Mn, REE), which decrease the values of unit-cell parameters.

The foraminifera and sponge spicules were detected only exceptionally and are clearly recycled because they are silicified, heavily corroded and virtually indeterminable.

In the electron microscope the polished sections of all concretions are structurally similar, i.e. microsparitic. They consist of very small aggregates of carbonates (complicated intergrowths of rhombohedrons), usually with subhedral shape, which are embedded in fine-grained matrix with a dominant proportion of apatite (rhodochrosite–apatite concretions) or clay minerals (siderite-rich concretions). Apatite is present only in the matrix and is extremely fine-grained. Exceptionally, its hypidiomorphic crystals are in size above 1 μm form also lath shaped crystals with a thickness of 2–3 μm in a length of up to 50 μm. However, this size prevented to gain precise EMPA-WDS analysis, since emission volumes (see Batanova et al. 2018) exceeded the volume of individual apatite grains. The results always included Si and Al, which we consider as contamination from other mineral grains. The matrix also contains grains of clastic admixture, especially mica, quartz and albitic plagioclase. Rare are framboidal pyrite, exceptional rounded grains of zircon and monazite. Often strongly corroded foraminifer shells are seen in the SEM, completely replaced and filled with Mn carbonates. The zoning of rhodochrosite is only very weak in the backscattered electron images. In rhodochrosite–apatite concretions, the centres of carbonate crystals are more likely to be richer in Mn and the margins in Ca and, to a smaller extent, also in Fe and Mg. However, the observed zoning is non-contrasting and is rather produced by the accumulation of submicrometre particles on the edges. For manganese-rich siderite concretions, zoning in back-scattered electrons (BSE) somewhat more pronounced and light cores are surrounded by darker rims. In addition, a discontinuous pale coating of up to 1.5 μm thickness is developed on the grain surface, which chemically corresponds to the middle part of the grain, mainly due to Fe/Mn distribution, lesser to Ca and Mg, which is also evident from EDS mapping (Fig. 5) and ternary plots (Fig. 6).

Electron microanalyses of carbonates are shown in Tables 1 and 2 and Fig. 6. It is evident that the carbonates of rhodochrosite–phosphate concretions belong to rhodochrosite type. The proportion of the rhodochrosite component is in the crystal centres around 75 %. The composition of minerals from the apatite group cannot be analysed with respect to their small grain size. Siderite-rich concretions consist of a substituted siderite of strongly variable composition. Compositionally in centres of grains belongs to siderite up to Mn-rich siderite. The composition of the carbonate component of the concretions is evident from the diagrams (Fig. 6), where the results of both WDS and EDS microanalyses are presented.

In the relatively rare fissures in concretions, only calcite was found, containing slightly increased Mn (max. 2 at. %) and Fe (max. 1 at. %).

Mineralogy of the weathering products

Most concretions at the Řepiště site is in some degree of alteration. The concretions composed of rhodochrosite and apatite show black coatings and alteration zones around small cracks as well as on the surface (Fig. 7A,B). Some of these concretions have a mosaic structure. The electron microscope shows that the black zones (Fig. 2A) are composed of porous pseudomorphoses of manganese oxides after rhodochrosite aggregates. Such pseudomorphs consist of a massive marginal zone of manganese oxides and central part with a cavity or Mn-carbonate residue (Fig. 7C,D). The altered parts of the concretions then exhibit an apparently cellular structure. Mn-oxides also fill the occasional hairline cracks in the centres of alternate zones in the concretions.

The predominant Mn-oxide has been identified as todorokite in some parts of samples on the basis of powder X-ray diffraction analysis, with possible addition of birnessite and *buserite*.

The present todorokite is clearly poorly crystallised, and the estimated size of the crystal domains is about 13 nm. Diffraction bands (110)+(001) with a *d* value between 9.797 and 9.624 Å and (200)+(002) with a *d* value of 4.898 to 4.812 Å are distinguishable. In the diffraction pattern, there is also a complex band between 36.4 and 38.6 °2θ, with many indistinguishable lines of todorokite. Birnessite is very likely to be present in strongly altered samples as well as *buserite*, a phase not accepted by the IMA. Their main diffraction lines (birnessite d (001)=7.228 Å and *buserite* d (001)=10.02 Å), however, both coincide with the lines of chlorite and muscovite. Todorokite presence could not be confirmed by EMPA-WDS analysis due to its very small size, number of inhomogenities (inclusions) and somehow spongy character (see Fig. 7D).

The predominant weathering product of siderite concretions is goethite, which produces pseudomorphoses after carbonates similar to todorokite but is more aggregated into kidney particles of submicrometre size. Todorokite in siderite concretions occurs in the surface layer of weathered zones and also in the thin fissures together with goethite.

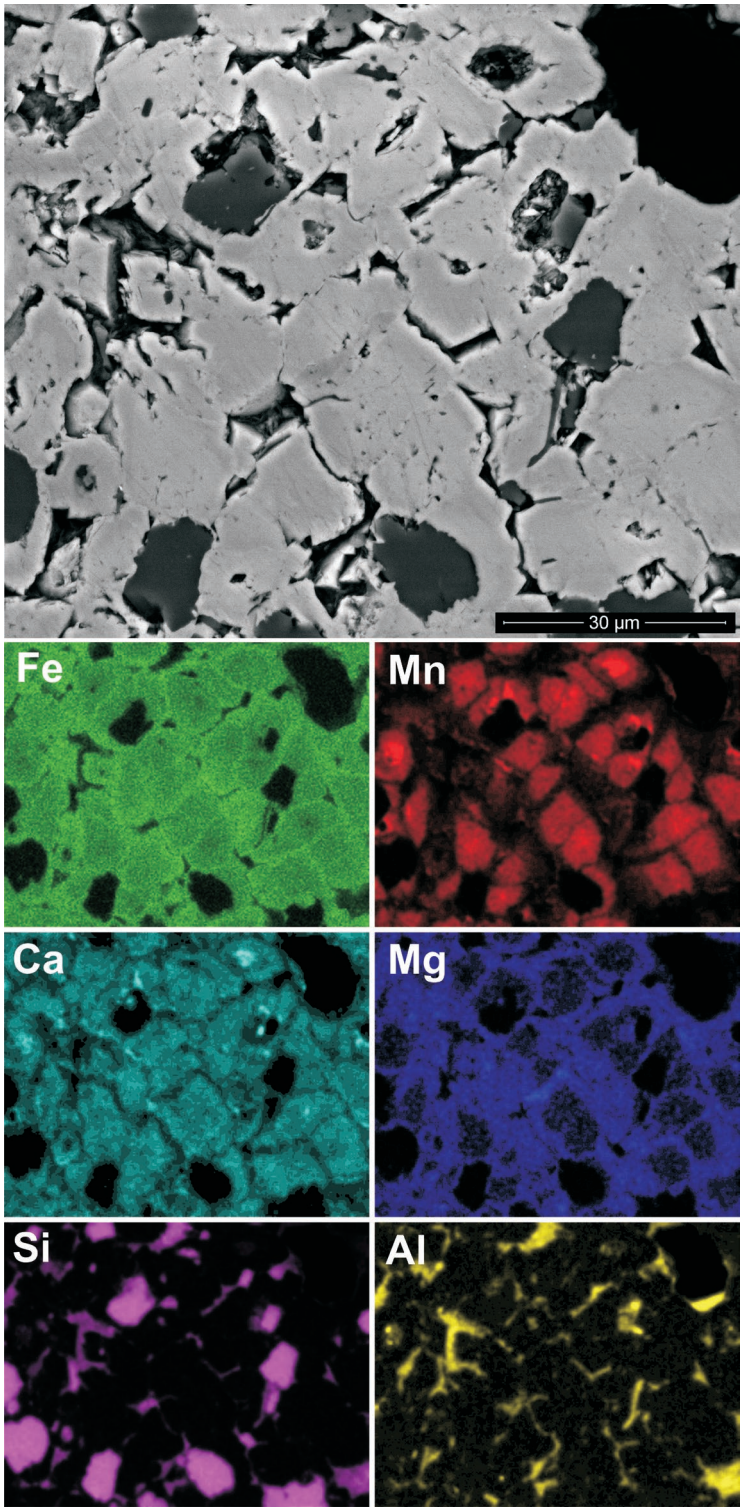

Fig. 5. BSE image of the polished thin section of the carbonate concretion from the Řepiště locality and EDS distribution maps of selected chemical elements. Fe, Mn, Ca, and Mg are major elements in microsparite carbonate. Grains rich in Si represent quartz, intergranular fills rich in Si+Al are clay minerals.

Interesting microscopic paragenesis of Se-rich minerals has been found in the fractures of sideritic concretions using SEM and EDS. In the fissures, a thin coating of Mn oxides is developed near the surfaces of concretion (Fig. 8A,B), and further to the centre, a coating of Fe-oxide/hydroxide, probably goethite, is developed. The presence of microcrystals of native selenium and clausthalite was found at the boundary of both zones, more often on the coating of

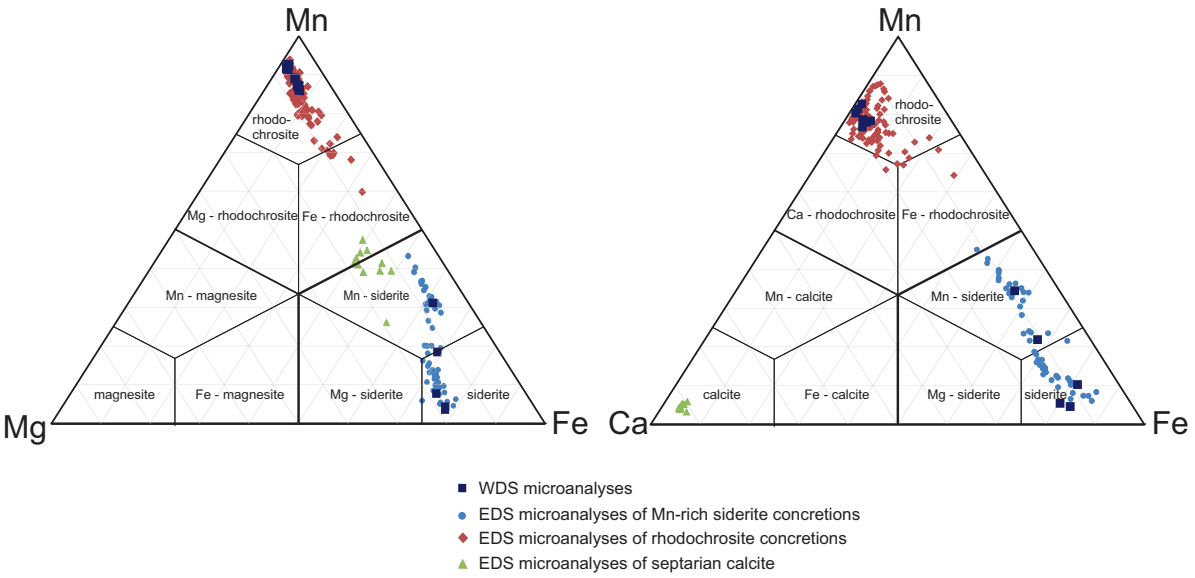

Fig. 6. Ternary plots of Trdlička & Hoffman (1975) showing the composition of carbonates (mol. %) of the studied concretions.

Table 1: WDS electron microanalysis of carbonate concretions from the locality Řepiště. The REP1 sample represents the phosphate–rhodochrosite concretion, and the REP3 sample represents the siderite to manganese-rich one. Note: b.d.l. = below detection limit.

	SiO_2	Al_2O_3	MgO	FeO	MnO	ZnO	CaO	SrO	BaO	PbO	Na_2O	K_2O	$CO_{2\ calc}$	total
	wt.%													
REP1/1	0.90	0.37	1.90	2.82	45.96	0.07	9.10	b.d.l.	b.d.l.	b.d.l.	0.06	0.07	39.49	100.73
REP1/2	1.12	0.50	1.86	0.84	47.68	0.05	8.81	0.04	b.d.l.	b.d.l.	0.18	0.12	39.09	100.28
REP1/3	0.31	0.11	1.89	0.87	49.56	0.02	7.76	b.d.l.	0.005	0.093	0.01	0.03	39.46	100.10
REP1/4	1.32	0.59	1.82	2.91	45.55	0.03	8.19	b.d.l.	b.d.l.	0.041	0.10	0.15	38.47	99.15
REP1/5	0.52	0.55	1.99	3.30	46.29	0.06	7.83	0.05	b.d.l.	0.005	0.08	0.02	39.12	99.80
REP1/6	2.28	0.95	1.73	2.16	45.79	0.01	8.37	b.d.l.	b.d.l.	b.d.l.	0.04	0.20	38.19	99.71
REP1/7	0.88	0.40	1.64	0.76	48.07	0.01	8.31	0.04	b.d.l.	b.d.l.	0.12	0.05	38.62	98.90
REP3/1	0.07	0.02	6.74	45.40	2.42	0.06	5.33	b.d.l.	0.002	0.087	0.02	0.00	40.91	101.07
REP3/2	0.18	0.04	6.40	43.89	2.87	0.08	6.00	b.d.l.	b.d.l.	0.009	0.01	0.02	40.41	99.91
REP3/3	0.69	0.40	6.63	43.10	5.21	0,03	3.41	0.02	b.d.l.	b.d.l.	0.04	0.08	39.55	99.13
REP3/4	0.71	0.46	2.45	33.37	19.44	0.03	4.11	0.02	b.d.l.	0.001	0.06	0.09	38.42	99.15
REP3/5	0.38	0.11	4.39	38.21	11.83	0.06	4.66	0.01	0.024	0.039	0.14	0.03	39.25	99.13

Table 2: Conversion of analyses to structural formulas and to molar proportions of carbonate end members. The contents of SiO_2, Al_2O_3, Na_2O and K_2O were excluded from the calculation, as their contents are most likely derived from clay mineral inclusions in carbonates. The ZnO, BaO and PbO contents are very low, close to the limit of detection, and were therefore excluded as well. The proportion of these elements after conversion is max. 0.001 *apfu*.

	Mg	Fe	Mn	Ca	C	magnesite	calcite	siderite	rhodochrosite
	atoms per formula unit					mol. %			
REP1/1	0.052	0.044	0.722	0.181	1.000	5.24	18.09	4.38	72.20
REP1/2	0.052	0.013	0.757	0.177	1.000	5.20	17.69	1.32	75.68
REP1/3	0.052	0.014	0.779	0.154	1.000	5.22	15.44	1.35	77.93
REP1/4	0.052	0.046	0.735	0.167	1.000	5.15	16.71	4.63	73.45
REP1/5	0.056	0.052	0.734	0.157	1.000	5.56	15.70	5.17	73.42
REP1/6	0.049	0.035	0.744	0.172	1.000	4.95	17.20	3.47	74.39
REP1/7	0.046	0.012	0.772	0.169	1.000	4.65	16.88	1.21	77.22
REP3/1	0.180	0.680	0.037	0.102	1.000	18.00	10.23	67.98	3.67
REP3/2	0.173	0.665	0.044	0.117	1.000	17.30	11.66	66.53	4.40
REP3/3	0.183	0.668	0.082	0.068	1.000	18.29	6.76	66.75	8.17
REP3/4	0.070	0.532	0.314	0.084	1.000	6.95	8.40	53.20	31.39
REP3/5	0.122	0.596	0.187	0.093	1.000	12.22	9.32	59.63	18.70

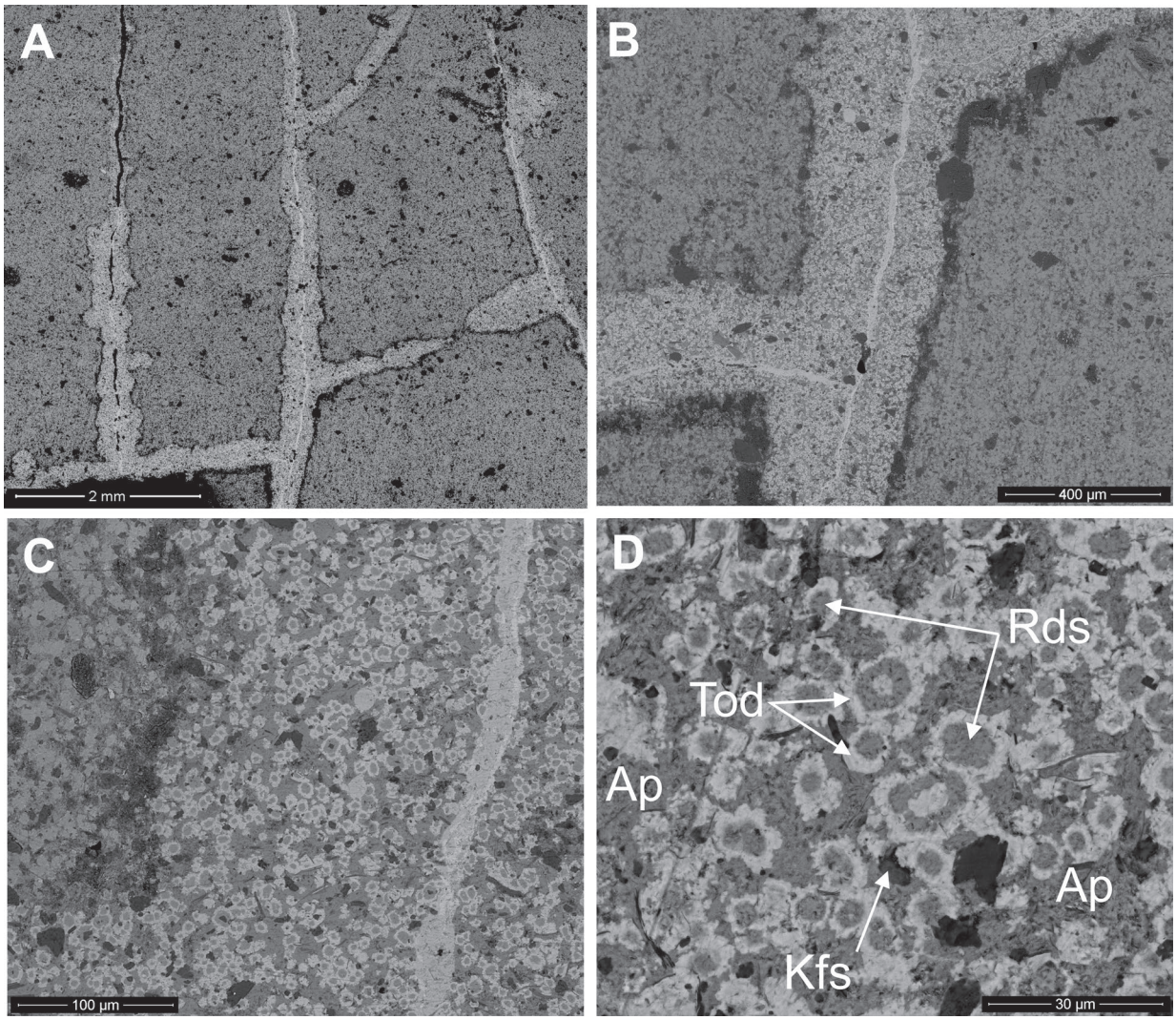

Fig. 7. BSE image of alteration of the rhodochrosite-phosphate concretion from the Řepiště locality. **A**, **B** — alteration zone (lighter grey) along the fissure; **C**, **D** — details of the previous pictures with concentrically zoned pseudomorphs of todorokite (Tod) after rhodochrosite (Rds) grains in the apatite (Ap) matrix with rare grains of K-feldspar (Kfs).

Fe-oxide. Determination of both phases is based only on semi-quantitative EDS microanalysis; wave dispersion microanalysis cannot be performed due to instability in the electron beam and very limited size. Native selenium forms aggregates of acicular crystals with a length of up to 20 µm and a thickness of up to 2.5 µm (Fig. 8C,D). Cubic clausthalite crystal aggregates have a size of up to 1 to 2.5 µm (Fig. 8E,F) and are often developed in the centres of selenium aggregates. EDS analyses for pure Se particles provide about 70–85 % Se content with the addition of environmental elements (Fig. 9); for clausthalite, the Pb+Se content is about 85 % (Fig. 9), and the ratio of these two elements is stoichiometric.

Geochemistry of the concretions

The bulk chemical composition was studied in three concretions and, for comparison, also from a sample of clay sediment enclosing the siderite concretions. The results of analyses (Tables 3 and 4) show considerable variability in the composition of the studied concretions, which is manifested both in the contents of the main components and trace elements, especially REEs. Table 3 shows the balance conversion to apatite and carbonate content neglecting the possible Mg, Fe and Ca content in the silicate component of the samples. However, due to the composition of the REP-d sample (claystone to clay from the direct surroundings), the Mg, Fe and Ca content of the silicates is negligible. The REP-a sample, according to its chemical composition, corresponds to a strongly substituted siderite; the REP-b sample consists of Ca-rich rhodochrosite, with a significant addition of apatite, and the REP-c sample is a phosphate with an admixture of calcite. Analysis of the REP-d sample corresponds to the composition of the surrounding clay sediment.

The total REE contents of the samples studied are highly variable and are clearly related to the proportion of the apatite component in the samples. The sample REP-c contains total of

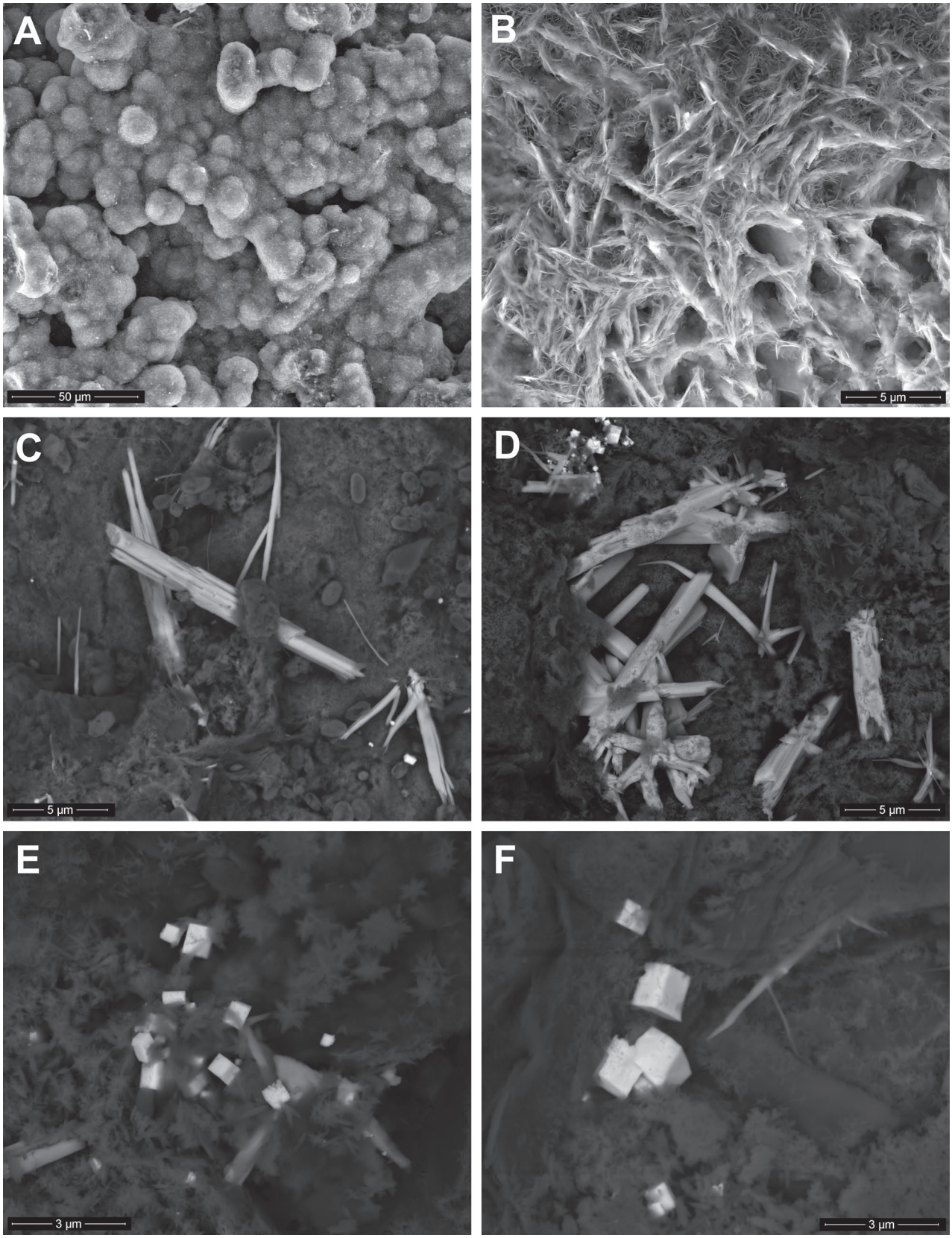

Fig. 8. BSE image of the selected minerals of concretions from Řepiště. **A**, **B** — foamy aggregate of todorokite; **C** — acicular native selenium on Fe-oxyhydroxide (goethite), oval shapes are Fe-oxidizing bacteria; **D —** acicular native selenium on Fe-oxyhydroxide (goethite); **E**, **F** - hexahedral clausthalite crystals with minor acicular native selenium on Fe-oxyhydroxide (goethite).

0.17 % REE at a P_2O_5 content of 26.5 %, the sample REP-b contains 0.04 % REE at a P_2O_5 content of 12.3 %. This can also be seen clearly in Fig. 10, where the distribution curves of the individual REE+Y, normalised to the average shale composition (PAAS standard; Taylor & McLennan 1995), are shown.

From the figure it can be clearly seen that the REE+Y for clay sediment (REP-d) is in accordance with the PAAS standard. The samples containing apatite and rhodochrosite (REP-b and especially REP-c) show strongly anomalous, normalised patterns with very pronounced enrichment of all REE+Y.

Compared to the chondrite composition, all studied samples exhibit a distinct depletion of Eu (Eu_n/Eu^*_n is between 0.55 to 0.76, with a minimum for REP-d). A cerium anomaly is not present (Ce/Ce^*_n is between 0.98 and 1.02). The chondrite-normalised values show anomalies, especially in the REP-d and REP-c, with significant enrichment of light and medium REE + Y.

Interesting is the anomalous high content of U (38 and 26 ppm, respectively), the reduced content of Th and, compared to the normal ratios in the crustal sediments, considerably enrichment in Se from samples with apatite (samples b and c).

The stable carbon and oxygen isotope ratios were studied in two carbonate samples (samples a REP-a and REP-b) and results are shown in Table 5. Samples are depleted in ^{13}C (−11.3 and −4.8 ‰ PDB, respectively) compared to the PDB standard. The $\delta^{18}O$ value approximately corresponds to the PDB standard (1.8 and 1.0 ‰ PDB, respectively) but is therefore significantly enriched by ^{18}O over SMOW (32.7 and 32 ‰ SMOW, respectively).

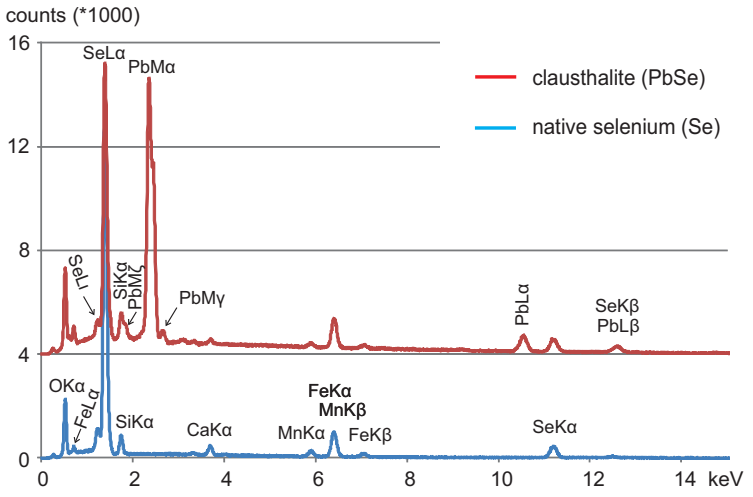

Fig. 9. EDS spectra of the investigated clausthalite and native selenium.

Table 3: Chemical composition (contents of the main components) of concretions from the locality Řepiště. Sample **a** represents a siderite with an increased proportion of Mn, Mg and Ca, sample **b** the phosphate rhodochrosite concretion, sample **c** belongs to phosphate, and sample **d** shows the composition of the clay surroundings of sample a.

	REP-a	REP-b	REP-c	REP-d
	%			
SiO_2	11.49	18.91	16.02	59.08
Al_2O_3	3.02	4.25	4.81	16.79
Fe_2O_3	37.11	6.99	4.11	6.64
MgO	4.77	1.05	0.59	2.52
CaO	4.68	20.97	36.86	1.72
Na_2O	0.2	0.38	0.41	0.98
K_2O	0.61	0.9	0.95	3.48
TiO_2	0.14	0.19	0.23	0.79
P_2O_5	0.11	12.34	26.53	0.13
MnO	7.24	18.56	3.19	0.12
Cr_2O_3	0.003	0.004	0.006	0.015
LOI	30.6	15.2	5.8	7.5
Total	99.973	99.744	99.506	99.765
TOT/C	9.46	3.15	0.93	0.59
TOT/S	< 0.02	0.02	0.04	< 0.02
apatite from P_2O_5	0.26	29.22	62.82	-
calcite	8.15	15.01	17.60	-
magnesite	9.98	2.20	1.23	-
siderite	53.85	10.14	5.96	-
rhodochrosite	11.73	30.08	5.17	-

Discussion

Concretions from the Subsilesian Unit of the Outer Western Carpathians were investigated at two localities in Podbeskydí area (Czech Republic) were found to be very variable, both mineralogically and chemically. They consist of a mixture of Ca-rich rhodochrosite and apatite in variable ratios and intensively substituted siderite. Structurally, the material corresponds to microsparite with an apatite or clay matrix. Concretion carbonates are inhomogeneous under X-ray diffraction. The carbonate zoning is insignificant. Overall zoning of rhodochrosite–apatite concretions (cores slightly enriched in Mn and margins in Ca, Fe and Mg) is the result of changing chemistry of sediment pore waters during the carbonate crystallisation. In manganese-rich siderite concretions, the Fe–Mn isomorphic distribution pattern was found. Considering the microsparitic character of the carbonates, the essentially homogeneous distribution their particle sizes and the signs of zoning, it is likely that in the concretions, the carbonate component recrystallised after initial precipitation, possibly by Ostwald ripening (Ostwald 1897; Kahlweit 1975).

Chemical analyses show a significant variability in the contents of the major constituents of the concretions. These components are a phosphate component (apatite), Ca-rich rhodochrosite, substituted siderite and clastic and clay

components. In addition, strong enrichment compared to PAAS was found in REE+Y (enrichment up to 50×, especially in MREE) and also in uranium in those concretions which contain significant amount of phosphatic component. Similar enrichment is known in number of sedimentary phosphates (Emsbo et al. 2015) and is interpreted by adsorption of REE^{3+} from aqueous fluids on apatite group minerals. Concretions composed of siderite are, in contrast to PAAS, clearly depleted on LREEs and MREEs. This depletion can be explained by larger ionic radius of $LREEs^{2+}$ compare to $HREEs^{2+}$ and a higher charge of $HREEs^{2+}$ than Fe^{2+}, which favours HREEs incorporation into the siderite (Bau & Möller 1992). The concretions lack cerium anomaly is due to origin in stabilised low oxidised environment, indicated also by formation of siderite itself, which demands highly reducing conditions. In opposite conditions Fe^{2+} would transform into Fe^{3+} and precipitate as iron oxides/hydroxides.

Table 4: Contents of trace elements in concretions and surrounding sediment from Řepiště.

	REP-a	REP-b	REP-c	REP-d
	ppm			
Ba	129	255	923	676
Ni	< 20	< 20	42	57
Sc	13	11	11	15
Be	8	4	< 1	1
Co	8	21.7	20.5	16.9
Cs	1.6	2.5	3.1	9.6
Ga	2.9	8.4	8.9	20.9
Hf	1	1	1.5	3.8
Nb	1.6	2.5	4.5	13.1
Rb	26.2	36.4	40.6	146.3
Sn	< 1	< 1	< 1	3
Sr	42.3	619.1	651.5	117
Ta	0.2	0.3	0.3	1
Th	2.3	2.7	4.3	12.5
U	1.5	37.9	25.8	3.1
V	50	43	60	142
W	1	0.6	0.6	2.2
Zr	38.1	40.5	55.1	153.5
Y	25.1	209.1	668.1	23.3
La	14.2	44.4	134.7	36.9
Ce	25	112.1	412.6	69.1
Pr	2.54	15.85	66.74	7.92
Nd	11.9	87	392.6	29.2
Sm	2.08	26.88	136.32	5.9
Eu	0.57	8.51	39.15	1.06
Gd	2.6	43.01	200.04	5.9
Tb	0.44	6.05	27.72	0.75
Dy	3.06	31.15	122.04	4.31
Ho	0.71	5.88	20.09	0.9
Er	2.4	13.24	39.83	2.87
Tm	0.32	1.36	3.76	0.41
Yb	2.3	7.16	19.13	2.7
Lu	0.41	0.93	2.38	0.42
Mo	1	2.6	3.5	0.1
Cu	5.5	11.6	9	31
Pb	10	31.9	32.9	16
Zn	78	67	63	95
Ni	14.3	18.1	43.5	47.6
As	1.7	3.4	3.6	2.3
Cd	< 0.1	0.2	0.2	< 0.1
Sb	< 0.1	0.2	0.3	0.1
Bi	< 0.1	0.1	0.4	0.3
Ag	< 0.1	< 0.1	0.1	< 0.1
Au	< 0.5	1.1	< 0.5	4.6
Hg	0.02	0.01	0.09	0.07
Tl	< 0.1	0.1	< 0.1	0.2
Se	< 0.5	1.4	4.9	0.5
total REE	68.53	403.52	1617.1	168.34

Carbonate concretions are clearly depleted in ^{13}C, while the ^{18}O corresponds to PDB but significantly are enriched in ^{18}O compared to SMOW. The values of $\delta^{18}O$ between 28 and 34 ‰ SMOW and values of $\delta^{13}C$ between −2.5 to −45 ‰ PDB correspond to marine early diagenetic carbonates (Raiswell & Fisher 2000; Kuleshov & Gavrilov 2001; Liu et al. 2019). The loss of ^{13}C and, respectively, the relative enrichment of ^{12}C, may correspond to suboxic diagenesis conditions (Morad & Al-Aasm 1997; Raiswell & Fisher 2000). Dissolved CO_2 was apparently not derived directly from seawater but was partly affected by the oxidation of biological material. The lower value can also be attributed to the presence of CO_2 derived from the anaerobic oxidation of methane (Raiswell & Fisher 2000). Therefore, the isotopic composition of the carbon and oxygen of the carbonate component of the concretions is from various sources. This is evidenced, inter alia, by the presence of foraminifera shells replaced and filled with rhodochrosite and is also influenced by the temperature.

The phase diagrams of the Fe/Mn-CO_3 system and kinetics of their precipitation (e.g., Curtis & Coleman 1985; Jensen et al. 2002) show that rhodochrosite is more stable than siderite at the same concentrations, even under slightly oxidising conditions (pε>3–4), when Fe precipitates in the form of oxides and Fe^{3+} oxyhydroxides, or is chelated with organic substances. Such conditions are indicated by the colour of

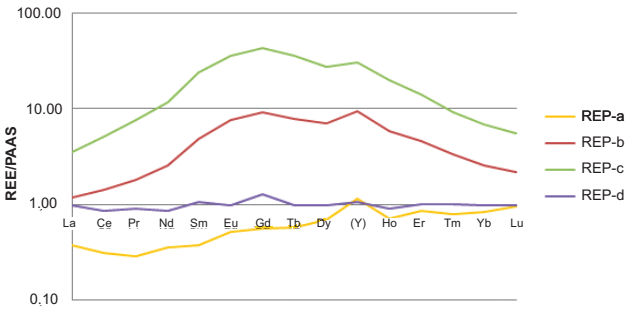

Fig. 10. PAAS-normalised REEs of the concretions and surrounding sediment. Normalization values after (Taylor & McLennan 1995).

Table 5: Isotopic composition of the investigated carbonate samples.

sample	d13C (‰ PDB)	d18O (‰ PDB)	d18O (‰ SMOW)
REP-a	−11.3	1.8	32.7
REP-b	−4.8	1.0	32.0

Subsilesian Unit's sediments, which is often red or contains red-brown-coloured strips (so-called variegated facies).

The weathering product of concretions with a significant content of Ca-rich rhodochrosite is todorokite in the form of aggregates with a pseudo-cellular structure. Microscopic mineralisation of native Se and clausthalite was observed in the fractures of the concretions formed by substituted siderite. It is the third find of native selenium associated with weathering in the Outer Carpathians (Matýsek & Skupien 2015; Szełęg et al. 2013) and first such case of clausthalite. Only few worldwide occurrences of clausthalite other than hydrothermal genesis were reported. To this group we can include clausthalite occurrences within the Proterozoic and Late Carboniferous metal-rich black shales (Coveney & Glascock 1989; Pašava et al. 1993), Proterozoic silicites (Scharm & Scharmová 1997), and some ot the U-V deposits of the Colorado Plateau (U.S.), where this phase is present both as primary and oxidized parts of the mineralized sandstones (Shawe 2011).

The formation of Se and possibly also selenides at the studied samples can be interpreted by precipitation on the redox interface between Mn^{2+}/Mn^{4+} and Fe^{2+}/Fe^{3+}, where selenites and selenates are strongly soluble but native selenium and selenides are extremely insoluble (Krivovichev et al. 2017). Thus selenium accumulates near the redox interface. Samples REP-b and REP-c (Table 4) show elevated concentrations of Se over the average Crust or PAAS content.

Conclusion

Concretions, not only in the Subsilesian Unit but also apparently throughout the Outer Western Carpathians (see Gucwa & Wieser 1978), cannot be described as siderite carbonates without microscopic study and macroscopically, individual types of concretions are not distinguishable. The only macroscopically visible clue to their composition may be their weathering display; (1) black coatings of Mn-containing oxides appear on the fissures of concretions with an increased Mn, (2) while brownish coatings of goethite might indicate siderite composition.

The formation of concretions with Mn-carbonates instead of more common siderite concretions can be explained by specific redox conditions of sedimentation and diagenesis.

Weathering of concretions is on the surface and along the fissures. While siderite-rich concretions produce goethite, rhodochrosite-rich concretions produce a cellular structure with todorokite, birnessite and *buserite* rims around carbonate cores. Fissure mineralisation contains unique association of goethite accompanied with native selenium and clausthalite.

Acknowledgments: This study was partly supported from the Czech Science Foundation (GAČR) project 19-17435S and used the infrastructure financed by Ministry of Education, Youth and Sports of the Czech Republic (project number 1406).

References

Batanova V.G., Sobolev A.V. & Magnin V. 2018: Trace element analysis by EPMA in geosciences: detection limit, precision and accuracy. *IOP Conference Series MAterials ans Engineering* 304, 012001. https://doi.org/10.1088/1757-899X/304/1/012001

Bau M. & Möler P. 1992: Rare earth element fractionation in metamorphogenic hydrothermal calcite, magnesite and siderite. *Mineralogy and Petrology* 45, 231–246. https://doi.org/10.1007/BF01163114

Baumann L.M.F., Birgel D., Wagreich M. & Peckmann J. 2016: Microbially-driven formation of Cenozoic siderite and calcite concretions. from eastern Austria. *Austrian Journal of Earth Sciences* 109, 211–232. https://doi.org/10.17738/ajes.2016.0016

Bojanowski M.J. 2014: Authigenic dolomites in the Eocene–Oligocene organic carbon-rich shales from the Polish Outer Carpathians: Evidence of past gas production and possible gas hydrate formation in the Silesian basin. *Marine and Petroleum Geology* 51, 117–135. https://doi.org/10.1016/j.marpetgeo.2013.12.001

Bojanowski M.J. & Clarkson E.N.K. 2012: Origin of siderite concretions in microenvironments of methanogenesis developed in sulfate reduction zone: an exception or a rule? *Journal of Sedimentary Research* 82, 585–598. https://doi.org/10.2110/jsr.2012.50

Bubík M., Franců J., Gilíková H., Otava J. & Švábenická H. 2016: Upper Cretaceous to Lower Miocene of the Subsilesian Unit (Western Carpathians, Czech Republic): stratotypes of formations revised. *Geologica Carpathica* 67, 239–256. https://doi.org/10.1515/geoca-2016-0016

Buriánek D., Bubík M. & Krejčí O. 2011: Carbonate concretions of the Moravsko-Slezské Beskydy Mountains (Czech Republic). *Geologické Výzkumy na Moravě a ve Slezsku* 18, 13–18 (in Czech with English abstract).

Comodi P., Liu Y., Zanazzi P.F. & Montagnoli M. 2001: Structural and vibrational behaviour of fluorapatite with pressure. Part 1: in situ single-crystal X-ray diffraction investigation. *Physics and Chemistry of Minerals* 28, 219–224. https://doi.org/10.1007/s002690100154

Coveney R. & Glascock M.D. 1989: A review of the origins of metal-rich Pennsylvanian black shales, central U.S.A., with an inferred role for basinal brines. *Applied Geochemistry* 4, 347–367. https://doi.org/10.1016/0883-2927(89)90012-7

Curtis C.D. & Coleman M.L. 1985: Controls on the precipitation of early diagenetic calcite, dolomite and siderite concretions in complex depositional seqences. In: Biddle K.T. & Christie-Blick N. (Eds.): Roles of organic matter in sediment diagenesis. *SEPM Special Publication* 38, 23–33. https://doi.org/10.2110/pec.86.38.0023

Dale A., John C.M., Mozley P.S., Smalley P.C. & Muggeridge A.H. 2014: Time-capsule concretions: Unlocking burial diagenetic processes in the Mancos Shale using carbonate clumped isotopes. *Earth and Planetary Science Letters* 394, 30–37. https://doi.org/10.1016/j.epsl.2014.03.004

De Craen M., Swennen R., Keppens E.M., Macaulay C.I. & Kiriakoulakis K. 1999: Bacterially mediated formation of carbonate concretions in the Oligocene Boom Clay of northern Belgium. *Journal of Sedimentary Research* 69, 1098–1106. https://doi.org/10.2110/jsr.69.1098

Dietrich R.V. 1999a: Carbonate concretions, part 1. *Rocks & Minerals* 74, 266–269. https://doi.org/10.1080/00357529909602551

Dietrich R.V. 1999b: Carbonate concretions, part 2. *Rocks & Minerals* 74, 335–340. https://doi.org/10.1080/00357529909602565

Dolníček Z., Kandrnál L., Ulmanová J., Vratislavská E. & Hojač P. 2019: Historical mining of pelosiderites at the locality Koryčanská cesta near Moravany, southern part of the Chřiby Mts. *Bulletin Mineralogie Petrologie* 27, 304–316 (in Czech with English abstract).

Dziubińska B. & Narębski W. 2004: Siderite concretions in Paleocene series of Polish part of the eastern flysch Carpathians. *Mineralogia Polonica* 35, 79–84.

Eliáš M. 1998: Sedimentology of the Subsilesian Unit. *Czech Geological Survey*, Praha, 1–48 (in Czech with English abstract).

Emsbo P., McLaughlin P.I., Breit G.N., du Bray E.A. & Koenig A.E. 2015: Rare earth elements in sedimentary phosphate deposits: Solution to the global REE crisis? *Gondwana Research* 27, 776–785. https://doi.org/10.1016/j.gr.2014.10.008

Friedman I. & O'Neil J.R. 1977: Compilation of stable isotope fractionation factors of geochemical interest. *U.S. Geological Survey Bulletin* 440, 1–12. https://doi.org/10.3133/pp440KK

Gucwa I. & Wieser T. 1978: Ferromanganese nodules in the Western Carpathian flysch deposits of Poland. *Rocznik Polskiego Towarzystwa Geologicznego* 48, 147–182.

Hodgson W.A. 1968: The diagenesis of spherulitic carbonate concretions and other rocks from Mangakahia group sediments, Kaipara Harbour, New Zealand. SEPM *Journal Sedimentary Research* 38, 1254–1263. https://doi.org/10.1306/74D71B45-2B21-11D7-8648000102C1865D

Jasionowicz J., Koszarski L. & Szymanowska F. 1959: Geological conditions of occurrence of phosphoritic concretions in the Węglówka variegated marls (Upper Cretaceous of the Middle Carpathian). *Kwartalnik Geologiczny* 3, 1016–1022 (in Polish with English summary + attachment).

Jensen D.L., Boddum J.K., Tjell J.C. & Christensen T.H. 2002: The solubility of rhodochrosite ($MnCO_3$) and siderite ($FeCO_3$) in anaerobic aquatic environments. *Applied Geochemistry* 17, 503–511. https://doi.org/10.1016/S0883-2927(01)00118-4

Kahlweit M. 1975: Ostwald ripening of precipitates. *Advances in Colloid Interface Science* 5, 1–35. https://doi.org/10.1016/0001-8686(75)85001-9

Kamran A., Schneider D., Roddatis V., Thiel V. & Hoppert M. 2020: Formation of siderite in microbial microcosms derived from a marine sediment. *Geomicrobiology Journal* 37, 475–485. https://doi.org/10.1080/01490451.2020.1725186

Krivovichev V.G., Charykova M.V. & Vishnevsky A.V. 2017: The thermodynamics of selenium minerals in near-surface environments. *Minerals* 7, 188. https://doi.org/10.3390/min7100188

Kuleshov V.N. & Gavrilov Yu.O. 2001: Isotopic composition ($\delta^{13}C$, $\delta^{18}0$) of carbonate concretions from terrigenous deposits in the Northern Caucasus. *Lithology and Mineral Resources* 36, 160–163. https://doi.org/10.1023/A:1004830602293

Liu A-Q., Tang D-J., Zhou L-M., Zhou X-Q., Shang M-H., Li Y. & Song H-Y. 2019: Growth mechanisms and environmental implications of carbonate concretions from ~1.4 Ga Xiamaling Formation, North China. *Journal of Palaeogeography* 8, 160–163. https://doi.org/10.1186/s42501-019-0036-4

Macoun J. (Ed.) 1989: Geological map of ČSR 1 : 50 000 with legend, Sheet 15-43 Ostrava. *Ústřední ústav geologický*, Praha, 1–78 (in Czech).

Macoun J., Šibrava V., Tyráček J. & Kneblová-Vodičková V. 1965: Quaternary of the Ostrava Region and the Moravian Gate. *Nakladatelství Československé akademie věd*, Praha, 1–420 (in Czech with English abstract).

Matýsek D. & Bubík M. 2012: Phosphate and pelocarbonate from pelitic rocks of the Subsilesian Unit at the R48 road constructions near Frýdek-Místek, Czech Republic. *Geologické Výzkumy na Moravě a ve Slezsku* 19, 88–91 (in Czech with English abstract).

Matýsek D. & Skupien P. 2005: Phosphorite concretions in the Upper Cretaceous of the Silesian Unit. *Geologické Výzkumy na Moravě a ve Slezsku* 12, 34–36 (in Czech with English abstract).

Matýsek D. & Skupien P. 2015: The origin of native selenium microparticles during the oxidation of sideritic mudstones in the Veřovice formation (Outer Western Carpathians). *Geologica Carpathica* 66, 303–310. https://doi.org/10.1515/geoca-2015-0027

Matýsek D., Jirásek J., Skupien P. & Thomson S.N. 2018: The Žermanice sill: new insights into the mineralogy, petrology, age, and origin of the teschenite association rocks in the Western Carpathians, Czech Republic. *International Journal of Earth Sciences* 107, 2553–2574. https://doi.org/10.1007/s00531-018-1614-x

Mavromatis V., Botz R., Schmidt M., Liebetrau V. & Hensen C. 2014: Formation of carbonate concretions in surface sediments of two mud mounds, offshore Costa Rica: a stable isotope study. *International Journal of Earth Sciences* 103, 1831–1844. https://doi.org/10.1007/s00531-012-0843-7

Menčík E., Adamová M., Dvořák J., Dudek A., Jetel J., Jurková A., Hanzlíková E., Houša V., Peslová H., Rybářová L., Šmíd B., Šebesta J., Tyráček J. & Vašíček Z. 1983: Geology of the Moravskoslezské Beskydy Mts. and the Podbeskydská pahorkatina Upland. *Academia*, Praha, 1–307 (in Czech with English summary).

Merlet C. 1994: An accurate computer correction program for quantitative electron probe microanalysis. *Microchimica Acta* 114, 363–376. https://doi.org/10.1007/BF01244563

Morad S. & Al-Aasm I.S. 1997: Conditions of rhodochrosite-nodule formation in Neogene–Pleistocene deep-sea sediments: evidence from O, C and Sr isotopes. *Sedimentary Geology* 114, 295–304. https://doi.org/10.1016/S0037-0738(97)00066-3

Moser L.K. 1875: Ein Beitrag zur mineralogischen Kenntniss des Teschner Kreises. In: III. Programm der k. k. Staats-realschule in Teschen am Schlusse des Schuljahres 1875/76. *Karl Prochaska*, Teschen, 15–42.

Muszyński M., Rajchel J. & Salamon W. 1978: Concretionary iron and manganese carbonates in eocene shales of the environs of Dynów near Przemyśl (Flysch Carpathians). *Mineralogia Polonica* 9, 111–123.

Nakada R., Shirai T., Takahashi S., Suzuki N., Ogawa K. & Takahashi Y. 2014: A geochemical constraint on the formation process of a manganese carbonate nodule in the siliceous mudstone of the Jurassic accretionary complex in the Mino Belt, Japan. *Journal of Asian Earth Sciences* 96, 59–68. https://doi.org/10.1016/j.jseaes.2014.08.032

Narębski W. 1960: Phosphorite concretions of the Węglówka variegated marls (Carpathian Flysch). *Acta Geologica Polonica* 10, 165–200 (in Polish with English abstract).

Ostwald W. 1897: Studien über die Bildung und Umwandlung fester Körper. *Zeitschrift für Physikalische Chemie* 22, 289–330. https://doi.org/10.1515/zpch-1897-2233

Pašava J., Sulovský P. & Kovalová M. 1993: Geochemistry and mineralogy of Proterozoic metal-rich black shales from the Bohemian Massif, Czech Republic, with a description of possible new molybdenum selenide and telluride phases. *Canadian Mineralogist* 31, 745–754.

Picha F., Stráník Z. & Krejčí O. 2006: Geology and hydrocarbon resources of the Outer Western Carpathians and their foreland, Czech Republic. In: Golonka J. & Picha J. (Eds.): The Carpathians and their foreland: Geology and hydrocarbon resources. *AAPG Memoir 84*, 49–175. https://doi.org/10.1306/985607M843067

Plet C., Grice K., Pages A., Ruebsam W., Coolen M.J.L. & Schwark L. 2016: Microbially-mediated fossil-bearing carbonate concretions and their significance for palaeoenvironmental reconstructions: A multi-proxy organic and inorganic geochemical appraisal. *Chemical Geology* 426, 95–108. https://doi.org/10.1016/j.chemgeo.2016.01.026

Raiswell R. & Fischer Q.J. 2000: Mudrock-hosted carbonate concretions: a review of growth mechanisms and their influence on chemical and isotopis composition. *Journal of the Geological Society* 157, 239–251. https://doi.org/10.1144/jgs.157.1.239

Rosenbaum J. & Sheppard S.M.F. 1986: An isotopic study of siderites, dolomites and ankerites at high temperatures. *Geochimica et Cosmochimica Acta* 50, 1147–1150. https://doi.org/10.1016/0016-7037(86)90396-0

Roth Z. & Matějka A. 1953: The Pelosiderites of the Moravosilesian Beskydy. *Nakladatelství Československé akademie věd*, Praha, 1–111 (in Czech with English and Russian abstracts).

Scharm B. & Scharmová M. 1997: Akcesorické minerály v proterozoických silicitických horninách z Kokšína u Mítova. *Bulletin mineralogicko-petrografického oddělení Národního muzea v Praze* 4-5, 113–120 (in Czech with English abstract).

Sellés-Martínez J. 1996: Concretion morphology, classification and genesis. *Earth-Science Reviews* 41, 177–210. https://doi.org/10.1016/S0012-8252(96)00022-0

Shawe D.R. 2011: Uranium-vanadium deposits of the Slick Rock District, Colorado. *U.S. Geological Survey Professional Paper* 576-F, 1–80.

Szełęg E., Janeczek J. & Metelski P. 2013: Native selenium as a by-product of microbial oxidation of distorted pyrite crystals: the first occurrence in the Carpathians. *Geologica Carpathica* 64, 231–236. https://doi.org/10.2478/geoca-2013-0017

Taylor S.R. & McLennan S.M. 1995: The geochemical evolution of the continental crust. *Reviews of Geophysics* 33, 241–265. https://doi.org/10.1029/95RG00262

Trdlička Z. & Hoffman V. 1975: Untersuchungen der chemischen Zusammensetzung der Gangkarbonate von Kutná Hora (ČSSR). *Freiberger Forschunghefte* C 321, 6, 29–81.

Wieser T. 1982: Manganiferous carbonate micronodules of the Polish Carpathian flysch deposits and their origin. *Mineralogia Polonica* 13, 25–42.

Yoshida H., Yamamoto K., Minami M., Katsuta N., Sin-ichi S. & Metcalfe R. 2018: Generalized conditions of spherical carbonate concretion formation around decaying organic matter in early diagenesis. *Scientific Reports* 8, 6308. https://doi.org/10.1038/s41598-018-24205-5